Application of Percolation Theory in Predicting Shape Distortion during Liquid-Phase Sintering

JIANXIN LIU, ANISH UPADHYAYA, and RANDALL M. GERMAN

This article shows how percolation theory provides a theoretical model for the onset of shape distortion in liquid-phase sintering. The model uses an equivalent bond number per grain, with bond strength depending on the relative intergrain bond size. Based on this study, shape distortion is resisted by a rigid compact, which depends on the solid grains forming an infinite chainlike structure that spreads throughout the system. A sufficient condition requires contiguity above a critical value to form an infinite chainlike structure. The critical value is near 0.38. This is in good agreement with experimental results obtained with the W-Ni-Fe system sintered both under microgravity and on Earth. The effect of the gravitational force on the sufficient condition to avoid shape distortion is not significant. The effect of gravitational field on shape distortion becomes apparent only after the start of distortion, determining the final profile of a distorted compact.

I. INTRODUCTION

MODELS that predict the properties of disordered media have emerged from percolation concepts first introduced by Broadbent and Hammersley.[1] Percolation theory predicts when a system is macroscopically connected. This macroscopic connectivity is important to many phenomena. Recently, German[2] introduced percolation concepts to describe liquid-phase sintering processes and shape distortion. It is postulated that if the solid phase is connected macroscopically, then shape retention is possible, otherwise the component distorts.

Liquid formation during sintering usually enhances densification. Traditional liquid-phase sintering begins by mixing two or more powders of differing compositions.[3] On heating, the powder with the lower melting point melts or reacts to form a liquid between the particles that engulfs the more-refractory phase. If the particle size is small, then the capillary forces from the wetting liquid enhance densification.[4]

Microgravity liquid-phase sintering provided a means to examine sintering distortion and microstructural changes under the condition of minimized gravity. At low solid contents, the compacts distort and spheroidize, since the surface tension exceeds all other forces in microgravity liquid-phase sintering.[5]

In ground-based sintering, gravity provides a progressive stress gradient on the powder compact that induces grain contact, settling, and anisotropic deformation (evident as shape distortion).[6,7,8] An "elephant-foot" shape is frequently observed for distorted W-Ni-Fe powder compacts. In addition, the solid and the liquid seldom have the same density. Hence, gravity induces microstructural separation gradients that result in nonuniform microstructures and properties in the sintered product.[7] The final microstructure consists of gradients which reflect the large density difference between the solid and liquid phases.[9] Gravity produces a systematic change in solid content, contiguity, connectivity, and grain size over relatively small distances.[10–13]

Shape distortion will be associated with microstructural parameter changes in this percolation mode. The dominant feature is the connection or bonding between neighboring grains. A sufficient level of bonding is necessary to form a rigid skeleton and inhibit shape distortion during liquid-phase sintering. This study addresses a critical condition *via* calculations based on percolation theory, to judge if a rigid skeleton is formed to resist shape distortion. The model is used to predict shape distortion under both microgravity and ground-based liquid-phase sintering conditions.

II. ELEMENTS OF PERCOLATION THEORY

The foundation of percolation theory is well explained in various references.[14–20] For the sake of clarity, some of the basic concepts are reviewed here before describing the application of percolation theory to liquid-phase sintering.

A. *Concept of Percolation*

Flory[19] and Stockmayer[20] used percolation to describe how small branching molecules reacted to form very large macromolecules. This polymerization process may lead to gelation, *i.e.*, to the formation of a very large network of molecules connected by chemical bonds, a key concept of percolation theory. Broadbent and Hammersley[1] developed it mathematically and first established the percolation theory.

Classical percolation theory centers around two problems.[15,21] In the bond percolation problem, the bonds of the network are either occupied, randomly and independently of each other with a probability of p, or are vacant, with a probability of $(1 - p)$. For a large network, this assignment is equivalent to removing a fraction $(1 - p)$ of all bonds at random. Two sites are called connected if there is at least one path between them consisting solely of occupied bonds. A set of connected sites bound by vacant bonds is termed a cluster. If the network is of very large extent and if p is sufficiently small, the size of any connected cluster is small. But if p is close to 1, the network should be entirely connected, apart from occasional small holes. At some well-defined value of p, there is a transition in the random network

JIANXIN LIU, Researcher, Mechanical Properties, ANISH UPADHYAYA, Researcher, Materials Development, and RANDALL M. GERMAN, Brush Chair Professor in Materials, are with The Pennsylvania State University, University Park, PA 16802-6809.

Manuscript submitted October 14, 1998.

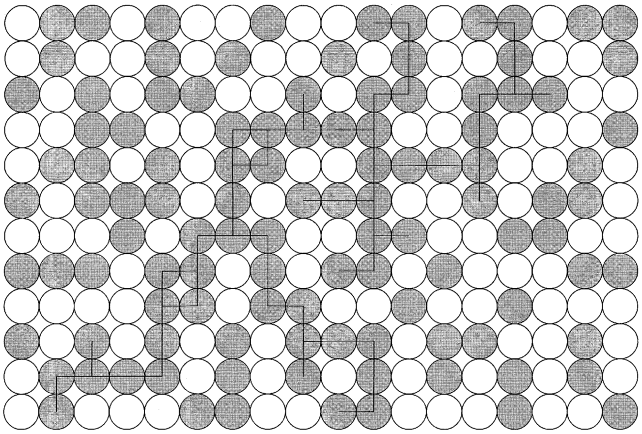

Fig. 1—Percolation on a two-dimensional square lattice. Dark circles indicate occupied sites, and white circles indicate empty sites. Two sites are called connected if there is at least one bond (between two occupied sites). An infinite cluster is indicated by heavy lines.

structure from a macroscopically disconnected structure to a connected one; this value is called the bond percolation threshold (p_{cb}). It is the smallest fraction of randomly occupied bonds below which there is no infinite cluster of occupied bonds.

Similarly, in the site percolation problem shown in Figure 1, sites of the network are occupied (dark circles), with a probability of p, or vacant (white circles), with a probability of $(1 - p)$. Two nearest-neighbor sites are considered to be connected if they are both occupied, and connected clusters on the network are again defined in the obvious way. There is a site percolation threshold (P_{cs}) above which an infinite cluster of occupied sites spans the network. Percolation problems generally depend on site and bond properties simultaneously.

Consider bond percolation on the square lattice defined by randomly occupying each edge (or bond) of the lattice with a given probability of p. Figure 2(a), based on Redner,[22] shows a two-dimensional 20×20 section of a square lattice whose edges are occupied with $p = 0.35$. From a geometrical point of view, there are two points that deserve emphasis. First, only small clusters up to a length scale denoted by the correlation length (ξ_p) dominate the lattice (the number of clusters with size $> \xi_p$ is exponentially small). Second, the clusters are disconnected; it is not possible to find a continuous path that traverses the lattice.

In Figure 2(c), a sample at $p = 0.65$ is shown. There now exists a single very large connected cluster which traverses the lattice. The correlation length, defined as the characteristic length scale of finite clusters, is, therefore, limited in this situation.

Intermediate to the situations depicted in Figures 2(a) and (c) is the percolation threshold, $p = p_c$. For the square lattice, a critical condition occurs at $p_c = 1/2$ (Table I). An example of such a critical state is shown in Figure 2(b), on which a percolating path is indicated. In particular, notice that there exist clusters of all length scales, and ξ_p approaches infinity. This singular behavior of ξ_p turns out to be crucial in understanding the physical properties of random media.

The derivation of the exact values for the bond percolation threshold and site percolation threshold has been possible for certain lattices. The percolation thresholds of three-dimensional networks have been calculated numerically by Monte Carlo simulations and other techniques. Table I compiles the current estimates of p_{cb} and p_{cs} for common two- and three-dimensional lattices. This table shows that the product of $B_c = Z \cdot p_{cb}$, the mean number of bonds to a given site, is essentially an invariant for percolation networks, where Z is the number of neighbors per grain. Note that Z differs from the coordination number N_c (the number of bonds per grain). Figure 3 shows the difference between Z and N_c in two dimensions; however, both quantities are used here to refer to three dimensions. The former is the number of nearest grains an arbitrary grain has, which may not be in contact with the reference grain; $Z = 6$. The latter is the number of grains exactly in contact with the reference grain; $N_c = 2$. Later, we will see that $N_c = Z \cdot p$, where p is the probability that a grain has bonds with neighboring grains. This implies that the mean number of bonds depends only on the dimensionality of the lattice and not on the specific lattice type.

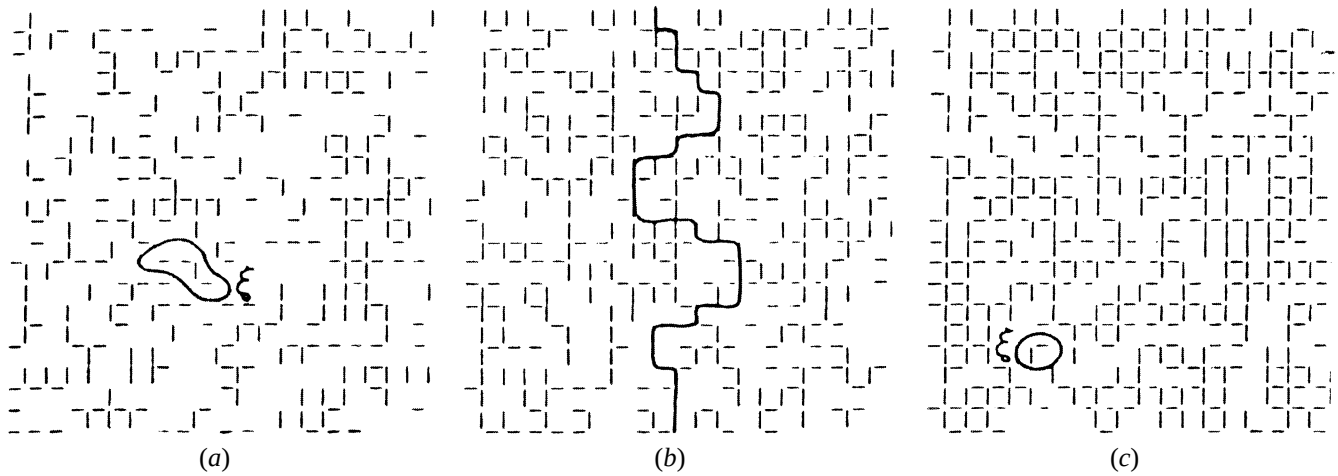

Fig. 2—(*a*) through (*c*) An intuitional bond percolation on a 20×20 section of the square lattice.[22]

Table I. Currently Accepted Values of the Percolation Thresholds[21]

Lattice	Dimension	Z	p_{cb}	$B_c = Z \cdot p_{cb}$	p_{cs}	$\phi_c = f_l \cdot p_{cs}$
Honeycomb	2	3	1 to 2 sin (π/18) $\approx$ 0.6527	1.96	0.6962	—
Square	2	4	0.5	2	0.5927	—
Triangular	2	6	2 sin (π/18) $\approx$ 0.3473	2.084	0.5	—
Diamond	3	4	0.3886	1.55	0.4299	0.146
Simple cubic	3	6	0.2488	1.49	0.3116	0.162
Bcc	3	8	0.1795	1.44	0.2464	0.168
Fcc	3	12	0.119	1.43	0.198	0.147

B. *Percolation Quantities*

In addition to the percolation thresholds, the topological properties of percolation networks are characterized by several other quantities. Percolation probability $P(p)$, correlation length, and the backbone fraction ($X^B(p)$) are most important in our study.

(1) Percolation probability is the probability that a randomly chosen bond or site belongs to the infinite cluster when the fraction of occupied bonds or sites is p.

$$P(p) + \sum_s s n_s = p \qquad [1]$$

where s is the length of an infinite cluster and n_s is the number of infinite clusters with a cluster length of s. The sum runs over all finite clusters and excludes the infinite cluster. This probability is zero for p values below the percolation threshold.

(2) Correlation length is the characteristic length scale used to describe finite clusters. When $p < p_c$, this is the typical size of the connected clusters. When $p > p_c$, it is defined as the characteristic length of finite clusters only, excluding the infinite clusters. This correlation length is crucial for many of our later discussions.

(3) Backbone fraction is the fraction of occupied bonds or sites in the infinite cluster which actually carry flow or current, since some of the bonds or sites in the cluster are dead-end and are not contributors to flow. The backbone of a percolating system plays a fundamental role in its transport properties, because the tortuosity of the transport paths is controlled by the structure of the backbone.

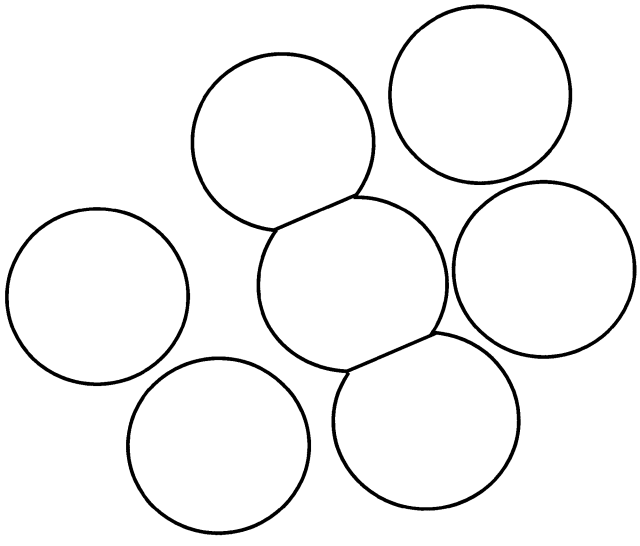

Fig. 3—A schematic showing the difference between definitions of coordination number in percolation theory and liquid-phase sintering. The reference grain in the center has six nearest grains, $Z = 6$, but only two contacting grains, $N_c = 2$.

To understand the backbone structure, it is helpful to begin with a two-dimensional rectangular lattice of squares with randomly removed sites, as sketched in Figure 4(a). The occupied dark squares are. conductive and occupied with a probability of p, and an empty square is an insulator, with a probability of $(1 - p)$, where p is termed the concentration of occupied sites. When voltage is applied to the top and bottom rows, an electric current can only flow between squares which have one side in common, not between corners. For a large lattice, we have zero conductivity if no infinite network of neighbors is present, that is, for $p < p_c$. The parameter p_c is a critical value, termed the percolation threshold. When $p < p_c$, there is no infinite cluster formed by occupied squares, while, when $p > p_c$, at least one infinite cluster exists. When p is appreciably larger than p_c, nearly all occupied squares are connected to form one infinite network. The conductivity ($C(p)$), as well as the fraction ($P(p)$) of sites in the infinite network, increase roughly linearly with concentration of p. At $p = 1$ we have, of course, $P(p) = 1$, and $C(p)$ reaches the bulk conductivity. If we set this bulk conductivity equal to unity, then $C(p = 1) = P(p = 1) = 1$. Because of the close relationship between the conductivity and percolation strength of an infinite cluster, it could be assumed that conductivity and percolation strength were proportional over the whole range of p. Last and Thouless[23] measured the electric current through a sheet of graphite paper with randomly punched holes. The result, shown schematically in Figure 4(b), indicates that $C(p)$ and $P(p)$ are not proportional. The conductivity *vs* concentration curve seems to end at the threshold with zero slope, while a plot of percolation strength *vs* concentration has infinite slope. The reason is that, even in the infinite cluster, many bonds carry no current, because they lead nowhere. These are called "dangling" or "dead-end" bonds. When we erase all the dangling bonds, we are left with the "backbone." Every internal bond on the backbone has at least two independent routes that lead from it to the edges of the cluster. Figure 5 shows a schematic of a liquid-phase sintering system. From the top to the bottom, some solid grains form a chain-like structure that is the same as an infinite cluster. The rest of the grains are probably agglomerated, but are

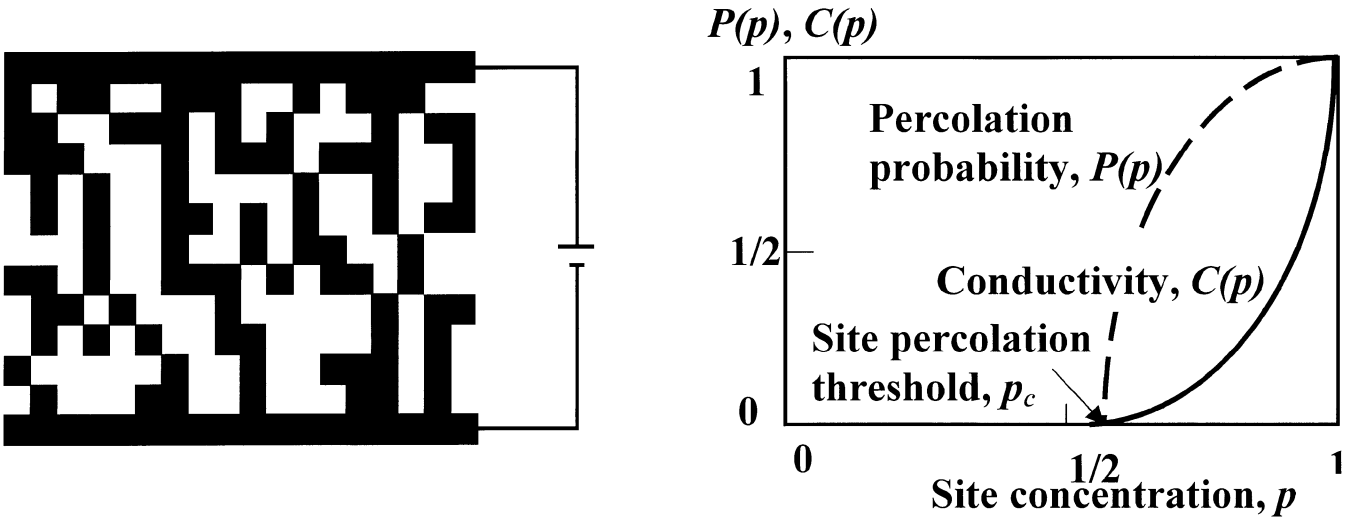

Fig. 4—(*a*) Percolation on a two-dimensional square lattice. The dark squares indicate sites occupied by a conductor. The white squares indicate empty sites. An electric current can only flow through the connected squares in the infinite cluster that is called a backbone; (*b*) a schematic that indicates that the conductivity $C(p)$ and the fraction of sites in the infinite network $P(p)$ increase with concentration p, but they are not proportional.

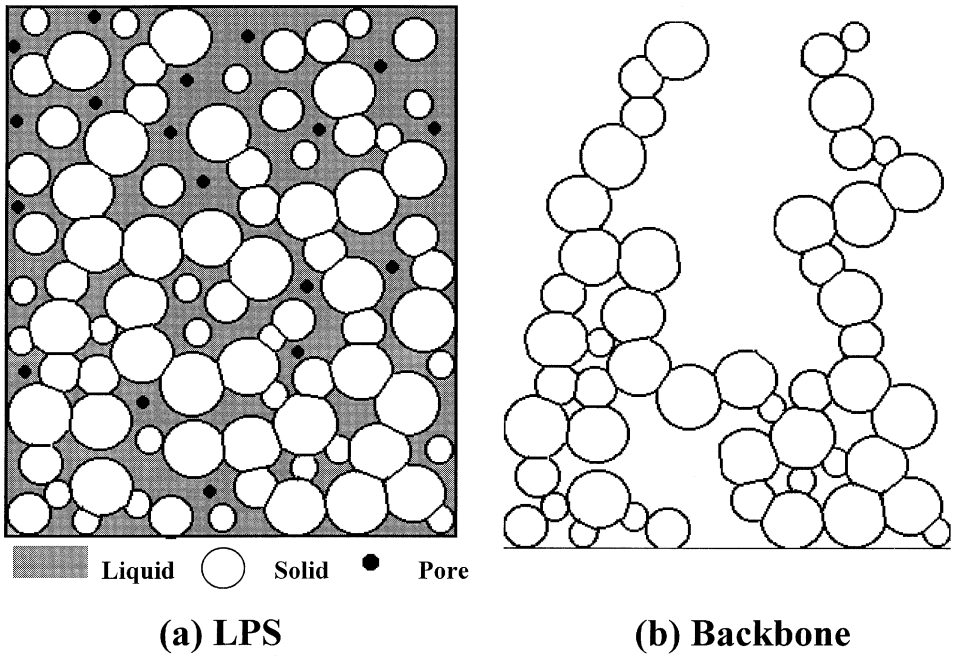

Fig. 5—(*a*) A schematic of a liquid-phase-sintered microstructure. From the top to the bottom, the solid grains form a chainlike structure that is the same as an infinite cluster. Some of the grains, which do not belong to the backbone chain, are dangling. (*b*) An image showing the backbone chain when these dead ends are removed.

not connected to this infinite grain chain. When the dead-ends and agglomerated grains are removed from Figure 5(a), we have the backbone chain, as shown in Figure 5(b).

Percolation quantities, such as percolation strength, correlation length, and backbone fraction, at a concentration of p, depend on the microscopic details of the system, such as its coordination number (nearest neighbors per site). But near the bond or site percolation threshold, most percolation quantities obey scaling laws that are largely insensitive to the network structure and its microscopic details. The quantitative statement of this insensitivity is that, near p_c, we have the following scaling laws:

$$P(p) \sim (p - p_c)^{\beta_p} \quad [2]$$

$$\xi_p(p) \sim |p - p_c|^{-\nu_p} \quad [3]$$

$$X^B(p) \sim (p - p_c)^{\beta_B} \quad [4]$$

Figure 6 shows the transition of percolation quantities at the

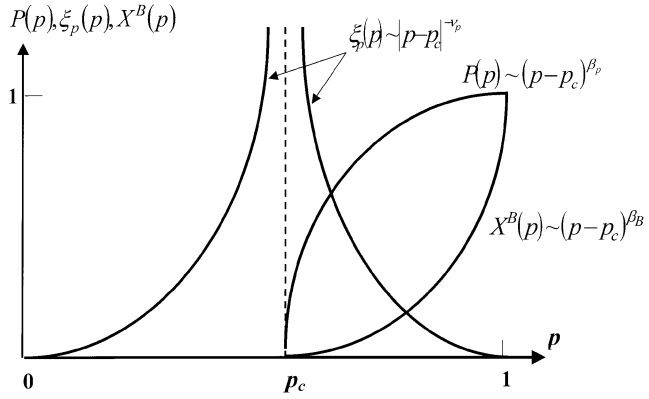

Fig. 6—Percolation quantities transition at the percolation threshold.

percolation threshold. The exponents β_p, ν_p, and β_B are completely universal, *i.e.*, they are independent of the microscopic details of the system and depend only on the dimensionality of the system. For three-dimensional networks, $\beta_B = 1.05$, $\beta_p = 0.41$, and $\nu_p = 0.88$.[21]

C. *Percolation in Random Networks*

Percolation in a topologically random network, in which the coordination number varies from site to site, is of great interest in our study liquid-phase sintering. There are at least three ways of realizing percolating continua.[24,25,26] If the system has a random distribution of spheres, similar to a liquid-phase sintering system, percolation is defined as the formation of an infinite cluster of touching or overlapping spheres. One of the most important discoveries for percolating continua is a critical occupied volume fraction (ϕ_c), defined by Scher and Zallen[27] as

$$\phi_c = p_{cs} f_l \qquad [5]$$

where f_l is the filling factor of a lattice, equal to volume-fractional density when each of its sites is occupied by a sphere, such as $f_l = 0.74$ for fcc, 0.68 for bcc, 0.52 for simple cubic, and 0.34 for diamond structures. Note that in bond percolation, the mean number of bonds to a given site (B_c) is essentially an invariant for percolation networks ($B_c = Z \cdot p_{cb}$). In site percolation, ϕ_c is a similar parameter to B_c, where ϕ_c corresponds to B_c and f_l corresponds to Z. The parameter ϕ_c appears to be an invariant of the system, with a value about 0.45 for $d = 2$ and 0.15 to 0.17 for $d = 3$, as listed in Table I. However, site percolation is difficult to apply in shape distortion. Shante and Kirkpatrik[28] generalized Scher and Zallen's idea to permeable spheres and showed that the average number of bonds per sites (B_c at p_{cb}) is related to ϕ_c by

$$\phi_c = 1 - \exp\left(-\frac{B_c}{8}\right) \qquad [6]$$

then the site percolation can be translated into a bond percolation system by Eq. [6]. Jerauld *et al.*[29] showed that, as long as the average coordination number of a random network and the coordination number of a regular network are about the same, many transport properties of the two systems are nearly identical.

D. *Homogeneity of Random Systems*

The total number of bonds or sites belonging to an infinite cluster ($M(L)$) depends on the volume of a system, L being the length scale of the volume (for a cubical-shaped network, the volume is L^3). The quantity $M(L)$ practically grows linearly with the volume L^3. We can define the average density of sites belonging to the infinite cluster as $P(p) = M(L)/L^3$, where $P(p)$ is independent of L and monotonically decreases as p decreases. However, the situation is very different for the probability of occupied bonds or sites very close to the percolation threshold, since $P(p)$ is not uniform. In this regime, the total number of bonds or sites belonging to an infinite cluster is given by

$$M(L, \xi_p) \sim \begin{cases} L^{D_c} & L < \xi_p \\ \xi_p^{D_c}(L/\xi_p)^d & L > \xi_p \end{cases} \qquad [7]$$

where d is the dimension of a system (for our case, $d = 3$). Generally, for any length scale where $L >> \xi_p$, a percolating system is macroscopically homogeneous. But, for $L << \xi_p$, the system is not homogeneous and the macroscopic properties of the system depend on L. Let D_c be the fractal dimension of the cluster. However, it is not a totally new quantity, since it is given by

$$D_c = d - \frac{\beta_p}{\nu_p} \qquad [8]$$

For $L > \xi_p$, we have $P(p) = M/L^d \sim \xi^{D-d} \sim (p - p_c)^{\beta_p}$ (same as Eq. [2]). For $L < \xi_p$, $M(L, \xi_p)$ grows as L^{D_c}, which implies that $P(p)$ is not constant, but rather decays as $L^{-\beta_p/\nu_p}$. When $L \to \infty$, then $P(p) \to 0$.

The correlation length decreases with a decrease of p when $p < p_c$. When $p > p_c$, the infinite cluster has a stronger propensity to absorb finite clusters. A large cluster has a greater possibility of being absorbed by an infinite cluster than a small one. So, the correlation length decreases as p increases over the percolation threshold.

The effect of finite system size manifests itself near the percolation threshold, where ξ_p is very large. However, we can treat a finite system as infinite as long as its length scale is $L >> \xi_p$, because the system is macroscopically homogeneous.

III. A PERCOLATION MODEL FOR LIQUID-PHASE SINTERING

Assume that a grain has Z nearest neighbors, but that not all of the neighboring grains necessarily form solid-solid contacts. To understand the connection with percolation, let us assume that the grains occupy the sites on a periodic lattice. The nearest grains (sites) form solid-solid contacts with a probability of p; if p is small, only small chains connecting a few grains are formed. As p increases, larger and larger chainlike structures are formed with a broad chain-size distribution. For $p > p_{cb}$, where p_{cb} is a characteristic value that depends on Z, an "infinite," continuous chain is formed. Thus, p_{cb} signals a connectivity transition: for $p > p_{cb}$, an infinite chain structure exists and the system is rigid (with possibly a few finite chains). The fraction of solid-solid contacts existing at a critical condition is the analogue of the bond percolation threshold.

Suppose the shape distortion depends on the presence or absence of an infinite continuous-grain network. The percolation threshold for shape distortion of a liquid-phase sintering system is, therefore,

$$p_{cb} = \frac{B_c}{Z} \quad [9]$$

where $B_c = 1.5$.[17,21] Besides the number of solid-solid contacts between an arbitrary grain and its nearest neighbors, we also need to know the bond strength to determine if a system remains rigid during liquid-phase sintering. So far, we have assumed that the percolation network consists of only two types of bonds: perfect bonds (occupied bond), which have the bond strength of unity, and unoccupied bonds, which have the bond strength of zero. In a liquid-phase sintering system, it is often the case that the occupied bonds are not perfect and have a bond strength less than unity. A higher coordination is needed if contacts between solid grains are weakly bonded. In such cases, a rigid infinite network for resisting shape distortion may depend on a combination of bond probability and bond strength.

If a bond is derived from the atomic bonding forces between contacting grains and the strength in unit area is σ_o, the bond strength is characterized by the bond area of a solid-solid contact, $\pi/4\sigma_o X^2$, where X is the neck diameter. A perfect bond is assumed to be equal to the force breaking a grain ($X \rightarrow G$), so the perfect bond strength is $\pi/4\sigma_o G^2$, where G is the grain diameter. The normalized bond strength (σ) is given by

$$\sigma = \frac{X^2}{G^2} \quad [10]$$

According to percolation theory, the average number of bonds per grain (sites) at p_{cb} is about 1.5 and is related to a critical volume fraction of 0.15 to 0.17, as expected from Eq. [6]. That was the result obtained by a random mixture of different spheres, for example, conducting spheres mixed with insulating ceramic spheres, which showed an onset of metallic conductivity at a critical volume-fractional density of the conducting spheres.[29]

Because the normalized perfect bond strength is unity, we replace B_c with a equivalent bond number (B_e) that has a normalized bond strength of σ, B_e being related to B_c by

$$B_c = B_e\sigma \quad [11]$$

Similar to Eq. [9], we have an equation for equivalent percolation threshold (p_{eb}) and equivalent bond number.

$$Zp_{eb} = B_e = \frac{B_c}{\sigma} \quad [12]$$

Now we have $N_c^* = B_e$, where the superscript asterisk indicates that the parameter is in the critical condition, for example, N_c^* is the critical coordination number defined for liquid-phase sintering. The parameter p_{eb} represents a rigid infinite network formed by weak bonds and relates to the equivalent network with p_{cb} of perfect bonds in a system. Supposing that p is the probability in bond percolation, then N_c ($N_c = Zp$) indicates the number of solid-solid contacts for a grain in three dimensions.

Contiguity (C_{ss}) is another parameter used to describe the mean solid-solid contact area of an individual grain as a fraction of total interfacial area. Obviously, the contiguity is dependent on bond number and bond strength (the area of a bond).

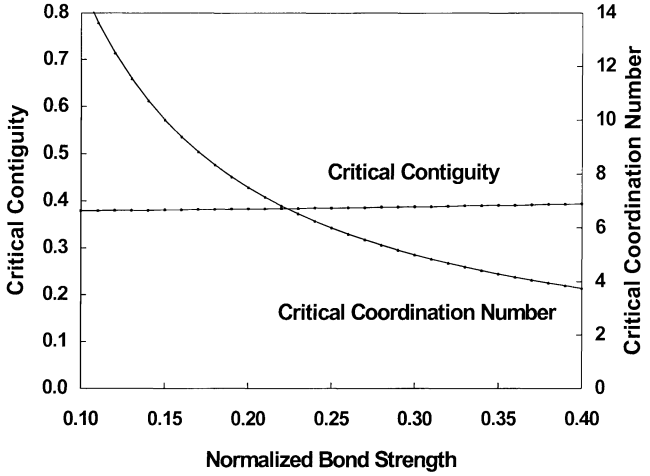

Fig. 7—Contiguity and coordination number (bond number) at the critical point of shape distortion, calculated based on the current model, showing a critical contiguity near 0.38 for no distortion.

$$C_{ss} = \frac{S_{ss}}{S_{ss} + S_{sl}} \quad [13]$$

where S_{ss} is the solid-solid surface area per grain and S_{sl} is the solid-liquid (matrix) surface area per grain. Considering a sphere of diameter G with N_c truncated contact flats, where the truncated flats are solid-solid contacts and the remaining area consists of solid-liquid surface, then S_{ss} and S_{sl} can be obtained by Eq. [14]:

$$S_{ss} = \frac{\pi X^2}{4} N_c \quad [14]$$

$$S_{sl} = \pi G^2 - \frac{\pi G(G - \sqrt{G^2 - X^2})}{2} N_c$$

On substituting Eq. [14] into Eq. [13],

$$C_{ss} = \frac{\frac{\pi X^2}{4} N_c}{\pi G^2 - \frac{\pi G(G - \sqrt{G^2 - X^2})}{2} N_c + \frac{\pi X^2}{4} N_c} \quad [15]$$

At the critical point of shape distortion, $p = p_{eb}$ and $C_{ss} = C_{ss}^*$.

$$C_{ss}^* = \frac{0.375}{1.375 - 0.75\,\frac{(1 - \sqrt{1 - \sigma})}{\sigma}} \quad [16]$$

Figure 7 shows the critical contiguity (C_c^*) and critical coordination number (N_c^*) plotted with the normalized bond strength, as calculated from Eq. [16] and [12], respectively. From Eq. [11] and $N_c^* \leq Z$, we have $\sigma = 1.5/N_c^* \geq 1.5/Z$. For a close packing of $Z = 12$, it gives a limit of $\sigma > 0.125$ and $C_{ss}^* > 0.38$. In practice, at least a coordination number of 4 is needed to hold the liquid-phase system rigidity for a random packing of spherical grains;[30] this corresponds to a contiguity of 0.39. Note that Eq. [16] and [12] are applied in the range of normalized bond strength between 0.125 and 0.375. Any extrapolation is inappropriate or gives

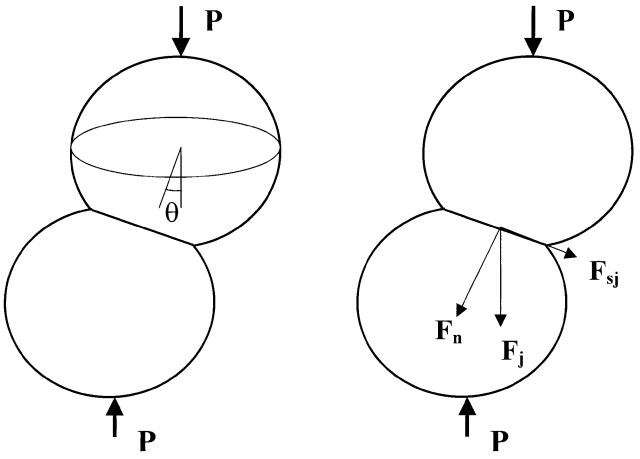

Fig. 8—A schematic of the force components induced by gravity on a neck.

incorrect conclusions. For example, an infinite critical coordination number will be obtained when the normalized bond strength approaches zero (Eq. [16]).

Contiguity is measured by quantitative microscopy on two-dimensional cross sections. The critical coordination number could not be measured directly. Furthermore, the critical contiguity is relatively invariant. This property highlights that the critical contiguity provides an efficient criterion for assessment of shape distortion other than the critical coordination number.

Based on the assumption of an equivalent bond number with weak bonding strength, the actual bond number is larger than 1.5 ($B_c = 1.5$). Also, the volume percentage of solid grains belonging to the infinite cluster at p_{eb} is larger than that expected at the percolation threshold.

IV. GRAVITY EFFECT ON SHAPE DISTORTION

During ground-based sintering of a cylindrical compact, the mean pressure induced by gravity (P) is proportional to the height of the compact,

$$P = \rho g y = (V_s\rho_s + V_l\rho_l)gy \qquad [17]$$

where ρ is the density; V is the volume fraction; subscripts l and s designate the liquid and solid, respectively; g is the gravitational acceleration; and y is the position from the top of the compact. The mean pressure is calculated based on the total cross-sectional area of the compact. In granular media, mechanical loading is primarily transmitted through intergrain contact. Hence, the pressure exerted on necks exceeds the mean pressure. Assuming that the force induced by gravity exerted on a neck j between two contacting grains in the backbone structure of the infinite grain chain is proportional to the product of the projected area ($1/4\pi X^2$) of the neck section resolved into the direction of gravity and the pressure distribution parameter (q), we get

$$F_j = \frac{\pi q X^2}{4}\cos\,\theta_j \qquad [18]$$

where θ_j is the angle between the gravity direction and normal direction for the neck section j. Figure 8 shows the force components on a neck schematically. The total force exerted on the necks located on the lower half of the reference grain is

$$\begin{aligned}\sum F_j &= \frac{\pi q X^2}{4}\sum_{1}^{ZX^B(p)/2}\cos\,\theta_j \\ &= \frac{\pi q X^2 Z X^B(p)}{8}\,\overline{\cos\,\theta} \\ &= \frac{\pi q X^2 Z X^B(p)}{16}\end{aligned} \qquad [19]$$

The factor $ZX_B(p)/2$ implies that only half of the grain contacts are taken into account. The parameter θ_j is a spatial angle and $\overline{\cos\,\theta} = 1/2$. Consider a hypothetical plane of area A and thickness G (G being the diameter of grains) inside the compact, vertical to gravity. The total force exerted on A is a summation of forces exerted on all individual grains located inside the volume $A \cdot G$. This force is equal to the pressure induced by gravity exerted on solid.

$$\begin{cases}\Sigma F = \dfrac{\pi q X^2 Z X^B(p)}{16} AG\,\dfrac{V_s}{1/6\,\pi G^3} = \dfrac{3ZX^B(p)qX^2AV_s}{8G^2} \\ \dfrac{\Sigma F}{A} = (V_s\rho_s + V_l\rho_l)gy\end{cases} \qquad [20]$$

Since $\sigma = (X/G)^2$,

$$q = \frac{8(V_s\rho_s + V_l\rho_l)gy}{3ZX^B(p)\sigma V_s} \qquad [21]$$

Substituting Eq. [21] in Eq. [18],

$$F_j = \frac{8(V_s\rho_s + V_l\rho_l)gy}{3ZX^B(p)\sigma V_s}\cdot\frac{\pi}{4}X^2\cos\,\theta_j \qquad [22]$$

As shown in Figure 8, F_j is divided into a shear force (F_{sj}) and a normal force (F_{nj}). They can be expressed as

$$\begin{cases}F_{sj} = F_j\sin\,\theta_j = \dfrac{2\pi X^2(V_s\rho_s + V_l\rho_l)gy}{3ZX^B(p)\sigma V_s}\sin\,\theta_j\cos\,\theta_j \\ F_{nj} = F_j\cos\,\theta_j = \dfrac{2\pi X^2(V_s\rho_s + V_l\rho_l)gy}{3ZX^B(p)\sigma V_s}\cos^2\,\theta_j\end{cases} \qquad [23]$$

The gravitational-force distribution indicates that the normal compressive force under gravity is greater in the necks with the normal direction parallel to the axial direction (gravitational direction) than in those parallel to the radial direction (nongravitational direction). The highest normal force occurs for necks oriented perpendicular to the axial direction and reduces to zero in the radial direction. The highest shear force is located at the necks with $\theta = 45$ deg, and the shear force is equal to zero in both the axial and radial directions. Shear force leads to the possibility of sliding between grains and combined rearrangement, depending on the bond strength of the contacts. The gravitational-force differences also exist along the axial direction because of the gravitational gradient and the gradient of solid volume fraction.

A normal force on the bonds creates a compressive stress gradient, such that there is enhanced material transport away from necks with the normal direction aligned parallel to the axial direction.[31–34] The consequence is more shrinkage in the axial direction than in the radial direction. However, the model presented in this article does not consider anisotropic shrinkage, but focuses on the critical microstructural condition for distortion. Therefore, normal compressive force is not considered because it does not break contacts between grains. Shear force leads to the possibility of sliding between

grains. The maximum shear force induced by gravity occurs at $y = h$ and $(\sin\theta \cdot \cos\theta)_{\max} = 1/2$, where h is the height of a compact.

$$F_{s,\max} = \frac{\pi X^2 (V_s\rho_s + V_l\rho_l)gh}{3ZX^B(p)\sigma V_s} \quad [24]$$

Under the gravitational field, the bond strength must be higher than that under microgravity to avoid shape distortion. Let a hypothetical bond strength (σ'), which is the bond strength $\pi/4\ \sigma_o X^2$ taken off the maximum shear force induced by gravity, instead of the bond strength $\pi/4\ \sigma_o X^2$.

$$\sigma' = \frac{\pi}{4}\sigma_o X^2 - F_{s,\max} \quad [25]$$

Thus, the percolation model in Section III is applicable for determining the onset of distortion under gravity. At the critical point of shape distortion, the critical coordination number and the critical contiguity are expressed as

$$N_c^* = 1.5\,\frac{\frac{\pi}{4}\sigma_o G^2}{\frac{\pi}{4}\sigma_o X^2 - F_{s,\max}} = \frac{1.5}{\sigma - \frac{4(V_s\rho_s + V_l\rho_l)gh}{3ZX^B(p)V_s\sigma_o}} \quad [26]$$

and

$$C_{ss}^* = \frac{0.375}{1.375 - 0.75\,\frac{(1-\sqrt{1-\sigma})}{\sigma} - \frac{4(V_s\rho_s + V_l\rho_l)gh}{3ZX^B(p)V_s\sigma_o\sigma}} \quad [27]$$

The backbone fraction is determined by Eq. [4]. For simplicity, we assume that the backbone fraction is a linear function of the probability p,

$$Z \cdot X^B(p) \sim (N_c^* - B_c) \quad [28]$$

Since $X^B(1) = 1$ when $N_c^* = Z$ ($p = 1$ and $B_c = 1.5$),

$$X^B(p) = \frac{N_c^* - 1.5}{Z - 1.5} \quad [29]$$

Equations [26] and [27] are simplified as

$$N_c^* = \frac{1.5}{\sigma - \frac{4(V_s\rho_s + V_l\rho_l)gh(Z-1.5)}{3Z(N_c^* - 1.5)\sigma_o V_s}} \quad [30]$$

and

$$C_{ss}^* = \frac{0.375}{1.375 - 0.75\,\frac{(1-\sqrt{1-\sigma})}{\sigma} - \frac{4(V_s\rho_s + V_l\rho_l)gh(Z-1.5)}{3Z(N_c^* - 1.5)V_s\sigma_o\sigma}} \quad [31]$$

When $h = 0$, the critical coordination number approaches $1.5/\sigma$ and the critical contiguity approaches that of Eq. [16]. When $h \neq 0$, the effect of gravity depends on the height of the compact, density, shear strength of the solid phase at the sintering temperature, solid volume fraction, and dihedral angle ($\sin\phi/2 = X/G \approx \sqrt{\sigma}$, where ϕ is the dihedral angle). When a compact is high, heavy, sintering at a high temperature (the bulk strength of the solid phase could be low at the temperature close to the melting point of the solid phase), a low solid volume fraction, and a low dihedral angle, the value of $4(V_s\rho_s + V_l\rho_l)gh(Z - 1.5)/[3Z(N_c^* - 1.5)V_s\sigma_o\sigma]$ may be not negligible.

For the W-Ni-Fe system sintering at 1500 °C, the density of solid tungsten is 19254 kg/m^3, the density of the liquid is estimated to be about 9000 kg/m^3, g is 9.8 m/s^2, and the height of the compact is 0.01 m. The solid strength is 25×10^6 N/m^2, estimated to be one-half of the yield strength at the sintering temperature.[35] The packing of nearest neighbors is assumed to be in the range from 9 to 12. For the 78 pct W-15.4 pct Ni-6.6 pct Fe alloy sintered at 1500 °C, the solid volume fraction is about 0.55, $4(V_s\rho_s + V_l\rho_l)gh(Z - 1.5)/[3\sigma_o V_s] \approx 0.0014$, and Eq. [30] and [31] become

$$N_c^* \approx 0.75 + \frac{0.75}{\sigma} + \frac{1}{2\sigma}\sqrt{2.25(1-\sigma)^2 + 0.0056\sigma} \quad [32]$$

and

$$C_{ss}^* = \frac{0.375}{1.375 - 0.75\,\frac{(1-\sqrt{1-\sigma})}{\sigma} - \frac{0.0014}{(N_c^* - 1.5)\sigma}} \quad [33]$$

For the 93 pct W-4.9 pct Ni-2.1 pct Fe alloy sintered at the same temperature, the solid volume fraction is about 0.8 and $4(V_s\rho_s + V_l\rho_l)gh(Z - 1.5)/[3\sigma_o V_s] \approx 0.0011$, given that

$$N_c^* \approx 0.75 + \frac{0.75}{\sigma} + \frac{1}{2\sigma}\sqrt{2.25(1-\sigma)^2 + 0.0044\sigma} \quad [34]$$

and

$$C_{ss}^* = \frac{0.375}{1.375 - 0.75\,\frac{(1-\sqrt{1-\sigma})}{\sigma} - \frac{0.0011}{(N_c^* - 1.5)\sigma}} \quad [35]$$

Figure 9 shows the critical contiguity, based on Eq. [33] and [35], and the critical coordination number, based on Eq. [32] and [34], for the 78 pct W-15.4 pct Ni-6.6 pct Fe and 93 pct W-4.9 pct Ni-2.1 pct Fe alloys, respectively. They are plotted with relative bond strength under the critical condition of liquid-phase sintering. Both critical values have very little differences between alloys and between microgravity sintering and ground-based sintering (compare to Figure 7).

The previous calculation shows that the critical contiguity for shape retention predicted from Eq. [31] is the same as that predicted from Eq. [16]. Gravity has no effect on the critical point of shape distortion. A possible explanation is that there is a dramatic decrease in the compact rigidity at the critical point. Above the critical contiguity, there is a percolation structure of solid contacts, while below that no percolation structure formed.

V. EXPERIMENTAL PROCEDURE

Commercial tungsten powder provided by Osram (Towanda, PA), nickel powder from Novamet (Wyckoff,

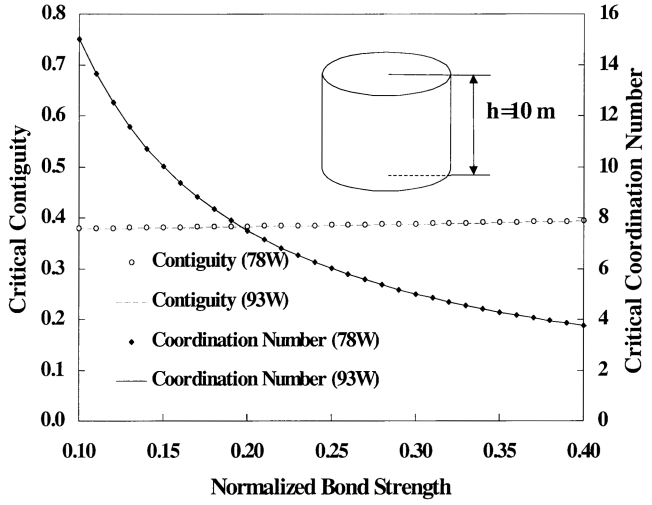

Fig. 9—The critical contiguity and coordination number for alloy 78W and alloy 93W ground-based sintered at 1500 °C. Results show that gravity has little effect on the critical point of shape distortion (compare with Figure 7).

NJ), and iron powder from International Specialty Products (Wayne, NJ) were used in microgravity liquid-phase sintering experiments. The powders were mixed to form alloys with 78, 83, 88, 93, and 98 pct tungsten (in wt pct) and the balance was nickel and iron in a 7:3 weight ratio. The mixed powders were cold-isostatically pressed at 210 MPa and solid-state sintered at 1400 °C for 3 hours in a dry hydrogen atmosphere. After presintering, the samples were machined into right-circular cylinders with a 10 mm height and diameter.

Microgravity sintering was performed in the large isothermal furnace aboard the space shuttle *Columbia*, as part of flight STS-65 in July 1994. The equivalent sintering was performed in a ground-based version of this furnace. In both cases, the samples were heated from ambient temperature, at an average rate of 18 °C/min, to 1500 °C. At 1500 °C, the temperature was held for 1, 15, or 120 minutes and then cooled at 3 °C/min to 1420 °C, below the solidus temperature. Sintering was carried out in vacuum. Subsequently, the furnace was shut off and allowed to cool to room temperature.

Measurements included dimensions, density, and microstructural analysis. Dimensional measurements were taken using a vernier caliper for the presintered samples and a coordinate measuring machine for the sintered samples. Presintered dimensions and weights were used to calculate presintered densities, and sintered densities were determined by the Archimedes' method. The microstructure parameters, solid volume fraction, and contiguity were measured to a 95 pct confidence level.

VI. EXPERIMENTAL RESULTS AND DISCUSSION

A. *Description of Shape Distortion*

In microgravity, the high-liquid-content compacts tended to spheroidize during liquid-phase sintering, as shown in Figure 10. It is necessary to determine shape distortion by comparing the sintered dimensions to the presintered dimensions. However, no comprehensive distortion parameter has been used to quantify shape distortion until now. The parameter used was proposed by Upadhyaya:[36]

$$\delta = [1 - a^b \cdot 10^{-c}]\ 100 \qquad [36]$$

In Eq. [36], a incorporates the aspect-ratio contribution and c consists of the radial and axial standard deviations normalized with the mean values.

$$a = \frac{h_o \bar{d}}{\bar{h} d_o}$$

$$b = \text{sgn}\left(\frac{\bar{h}}{h_o} - \frac{\bar{d}}{d_o}\right) \qquad [37]$$

$$c = \frac{\sigma_d}{\bar{d}} + \frac{\sigma_h}{h}$$

where h_o and d_o are the compact height and diameter, respectively, before sintering. The terms $\bar{h}$ and $\bar{d}$ are the average compact height and diameter, respectively, after sintering. The terms σ_d and σ_h are the measured standard deviation of the diameter and height, respectively. This distortion parameter (δ) varies in the range from 0 to 100. The larger the deviation from the sintered compact size, which is expected from isotropic shrinking, the larger is the distortion. For no distortion the shape change is isotropic and δ approaches 0. Table II lists the quantified shape-distortion parameter.

B. *Microstructural Changes*

Table II also lists the contiguity and solid volume fraction *vs* sintering time for the five alloys. Contiguity largely depends on the volume fraction of solid. In the 83 pct W alloy, the solid loading is higher than in the 78 pct W alloy, but, because of separation, the volume fraction of solid tungsten grains is almost the same as in the 78 pct W alloy. Both alloys have the same levels of contiguity.

Contiguity initially varies with sintering time. This is attributed to a change in the solid-liquid surface energy as the liquid composition changes during dissolution, spreading, and penetration of grain boundaries.[37] After prolonged sintering, the contiguity approaches a constant value, except for the 88 pct W alloy.

Because all the samples were sintered at the same temperature and had the same composition of liquid phase, the dihedral angle was constant. An average dihedral angle of 55 deg was measured from the samples of microgravity sintering, which is higher than that measured from the samples of ground-based sintering, the latter ranging from 25 to 52 deg.[3,5]

C. *Distortion Criterion*

For the 88 W alloy sintered at 1500 °C, sample distortion increases with the sintering time; Figure 10 shows the distortion for microgravity sintering. The distortion parameter ranges from 6.38 at the beginning to 38.32 after 120 minutes of sintering. Microstructural measurements give the highest contiguity of 0.36 after 15 minutes of sintering. The 93W alloy sintered at 1500 °C for 120 minutes shows no distortion. The contiguity is 0.41 for microgravity sintering and 0.418 at the top and 0.392 at the bottom for the ground-based

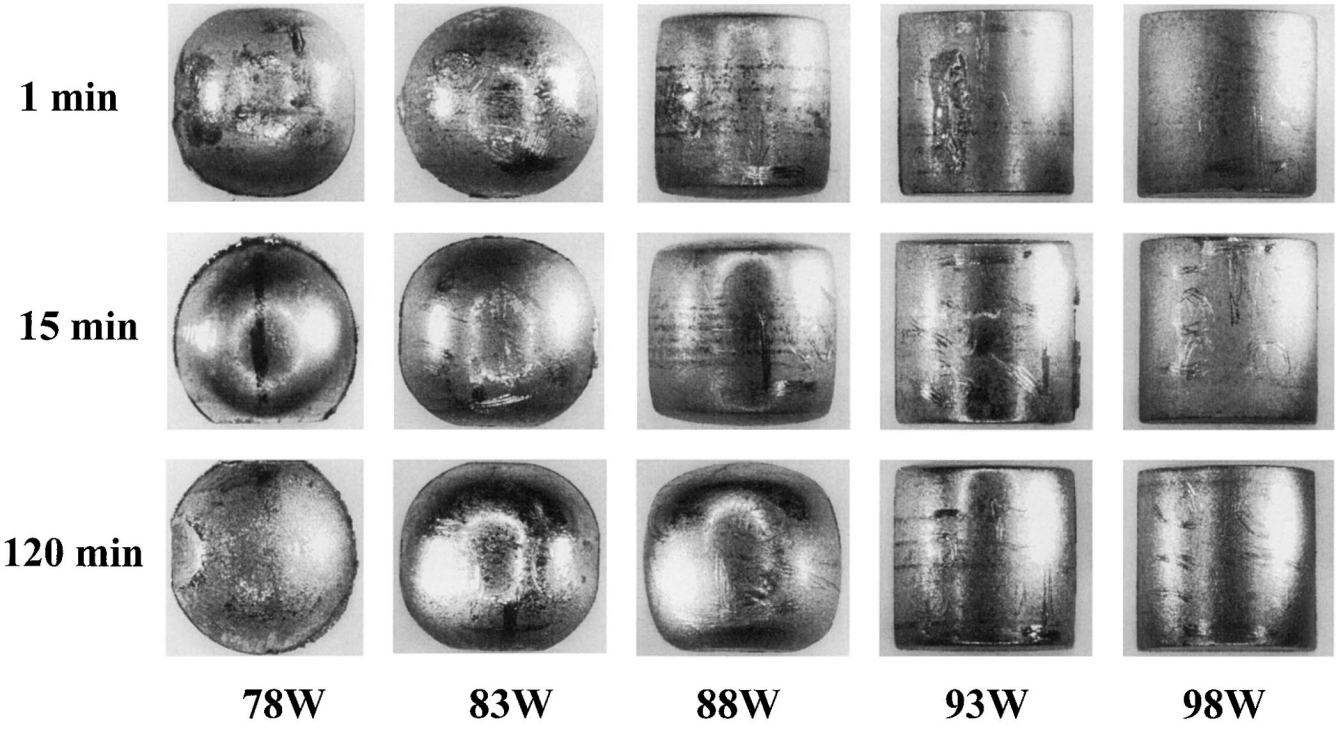

Fig. 10—Postflight shapes after microgravity sintering following 1, 15, or 120 min at 1500 °C.

sintering sample, respectively. Other liquid-phase sintering alloy systems are listed in Table III, based on the results of Upadhyaya.[36] The samples with contiguity below the critical value slumped, while the samples with the contiguity over the critical value resisted distortion.

This evidence shows that there is a sufficient condition for no shape distortion in liquid-phase sintering: when the contiguity is larger than the critical value, no distortion occurs. The theoretical value is near 0.38.

D. *Microstructural Description* via *Percolation Theory*

Contiguity increases with the increasing volume fraction of solid and dihedral angle. An empirical relation can approximate this behavior:[30]

$$C_{ss} = V_s^2(0.43 \sin \phi + 0.35 \sin^2 \phi) \qquad [38]$$

Based on Eq. [38], we can predict shape distortion simply from the solid volume fraction when the dihedral angle is known.

Percolation theory also gives us a microstructural description of a disordered system. In the case of perfect bonding between grains, when the average number of contacts per grain exceeds B_c ($B_c = 1.5$ for three dimensions), a continuous chainlike structure is expected. Furthermore, the probability of grains belonging to the infinite network calculated by Eq. [6] depends on the system size. At the percolation threshold, the correlation length is infinite, while the percolation strength decays as $L^{-\beta_p/\nu_p}$, as shown by Eq. [7]. Here, L is the system size and $\beta_p/V_p = 0.466$. When L is equivalent to 100 grains, $P_p(p) \sim 0.12$, while, if L is equivalent to 1000 grains, then $P_p(p) \sim 0.04$. In a very large system, the percolation strength will approach zero. However, for a liquid-phase sintering system, the bond strength is lower than perfect($(X/G)^2 < 1$). For example, in the 88 pct W alloy microgravity sintered at 1500 °C for 15 minutes, the average bond number per grain is 5.7, estimated from the connectivity in two-dimensional metallographic cross section. The correlation length is

$$\xi_p(p) \sim |p_{eb} - p_{cb}|^{-\nu_p} = \left(\frac{Z}{B_e - B_c}\right)^{0.88} = \left(\frac{14}{5.7 - 1.5}\right)^{0.88} = 2.88 \qquad [39]$$

The system is homogeneous and independent of the system size, because the sample is much larger than the grain diameter. The percolation probability $P(p)$ is calculated to be $2.88^{-0.466} = 0.61$ *via* Eq. [7]. As mentioned in Section II–B, the percolation probability is the probability that a randomly chosen bond or site belongs to the infinite cluster. Using Shante and Kirkpatrik's equation[28] (Eq. [6]), we have a critical solid volume fraction of 51 vol pct. Since the actual solid volume fraction is 75 vol pct for the 88 pct W alloy at 1500 °C, the equivalent site probability or site percolation threshold (p_{es}) is 0.68 (based on Eq [6]). The site percolation probability is given by

$$P_s(p) \sim (p_{es} - p_{cs})^{\beta_p} = \left(\frac{\phi_e - \phi_c}{V_s}\right)^{0.41} = \left(\frac{0.68 - 0.17}{0.75}\right)^{0.41} = 0.85 \qquad [40]$$

where subscript s represents the site percolation. The calculation shows that about 85 pct of the solid belongs to

Table II. Measured Distortion Parameters and Microstructural Parameters on W-Ni-Fe Powder Compacts Sintered at 1500 °C under Microgravity and Gravity*

Alloy	Sintering Time, Min	Distortion Parameter, Pct		Solid Volume Fraction, Pct			Contiguity, Pct		
					Ground Based			Ground Based	
		Microgravity	Ground Based	Microgravity	Top	Bottom	Microgravity	Top	Bottom
78W	1	43.99	slumped**	55.47	55.52	66.77	21.26	15.57	25.06
				(1.88)	(1.97)	(0.70)	(5.70)	(6.29)	(3.74)
	15	45.21		54.30	56.49	67.95	23.03	14.73	22.26
				(1.41)	(1.40)	(2.14)	(4.20)	(9.49)	(3.49)
	120	48.30		54.69	61.85	73.72	20.92	14.47	22.07
				(1.65)	(0.97)	(1.17)	(4.88)	(7.54)	(2.56)
83W	1	51.45	slumped**	56.67	53.53	65.49	17.89	15.33	24.44
				(1.32)	(1.63)	(1.98)	(4.84)	(5.66)	(3.64)
	15	45.06		53.42	56.73	62.82	18.14	19.66	26.10
				(2.30)	(1.43)	(1.59)	(4.84)	(5.57)	(4.44)
	120	42.73		54.67	64.96	70.41	17.22	24.68	28.18
				(2.37)	(0.45)	(1.05)	(4.51)	(3.73)	(3.09)
88W	1	6.38	slumped**	70.50	76.92	76.60	25.40	35.28	32.05
				(1.05)	(1.59)	(1.02)	(3.16)	(2.38)	(1.79)
	15	10.68		74.75	72.54	72.22	36.12	24.59	26.48
				(0.93)	(1.00)	(1.04)	(2.39)	(3.10)	(3.77)
	120	38.32		76.08	71.58	74.47	17.77	23.40	26.68
				(0.97)	(1.65)	(0.92)	(4.88)	(4.77)	(3.90)
93W	1	no distortion		86.07	84.42	83.23	51.45	49.88	44.60
				(1.24)	(0.57)	(0.62)	(1.66)	(1.80)	(1.26)
	15			86.25	80.45	80.88	44.08	47.25	43.79
				(0.83)	(1.57)	(0.60)	(1.49)	(2.65)	(1.52)
	120			85.42	83.48	83.76	40.59	41.76	39.16
				(1.17)	(1.15)	(0.91)	(3.28)	(2.91)	(3.14)
98W	1	no distortion		95.33	94.23	95.51	72.73	72.14	73.56
				(0.61)	(0.86)	(0.49)	(1.01)	(1.03)	(1.13)
	15			97.00	95.94	94.23	79.03	75.57	71.50
				(0.58)	(0.49)	(0.54)	(1.18)	(0.99)	(1.48)
	120			93.93	94.76	94.02	69.23	65.73	69.38
				(0.34)	(0.84)	(0.45)	(1.26)	(1.19)	(1.12)

*Data inside parentheses are coefficients of variation.
**Did not measure.

Table III. Liquid-Phase-Sintered Alloy Systems Show No Slumping Occurred When the Contiguity Values Were Larger Than the Critical Value, While Slumping Was Observed in Samples Where the Contiguity Was Less Than the Critical Value[36]

Alloy	W-7Ni	W-25.6Ni-6.4Cu	W-15Cu	Mo-20Ni	Mo-25Cu	Mo-24Cu
Sintering condition	1540 °C, 30 min	1400 °C, 30 min	1400 °C, 30 min	1500 °C, 30 min	1500 °C, 30 min	1400 °C, 30 min
Solid content, pct	70 ± 3.2	50 ± 2.5	70 ± 5.1	62	65	50 ± 1.7
Grain size, μm	35 ± 5.6	10 ± 4.2	5 ± 3.0	41	4	10 ± 3.5
Connectivity, C_g	0.2 ± 0.25	2.1 ± 0.21	4.2 ± 0.28	1.2	5.5	3.2 ± 0.18
Dihedral angle, ϕ	27 deg ± 6.5 deg	40 deg ± 5.1 deg	92 deg ± 8.1 deg	12 deg	95 deg	100 deg ± 5.6 deg
Coordination number, N_c	1.26	9.03	8.59	16.88	10.97	6.14
Contiguity, C_{ss}	0.15 ± 0.11	0.22 ± 0.03	0.61 ± 0.20	0.13	0.62	0.47 ± 0.05
Sintered density, pct theoretical	98	91	96	84	75	88
Description of sample	slumps	slumps	no slumping	slumps	no slumping	no slumping

the infinite chain and that only about 15 pct is not connected. The solid volume fraction of the 88 pct W alloy at 1500 °C is 75 vol pct at the sintering temperature, where 64 vol pct belongs to the infinite grain chain; therefore, only 11 vol pct of grains are not connected to the infinite chain. This 11 vol pct is constrained in the network of the infinite chain. It can be seen that the volume percentage of solid belonging to the infinite chain is much larger

than expected at the theoretical percolation threshold with perfect bond strength.

VII. SUMMARY

Percolation theory provides a theoretical base to predict shape distortion in liquid-phase sintering *via* the modified equivalent percolation threshold. Distortion is resisted if grains form a rigid infinite chainlike structure that spreads throughout the structure. The rigid infinite chainlike structure depends on the formation of solid-solid contact between grains and the bond strength (which depends on the relative intergrain bond size). The approach gives a distortion-resistant condition decided by contiguity only. When the contiguity of a liquid-phase sintering system is larger than the critical value (near 0.38), no distortion occurs.

The effect of the gravitational force is not significant, based on the current calculations. At the critical point where distortion might occur, grains remain in contact and the shear yield strength of tungsten is high enough to resist the effect of gravity. For smaller compacts, the effect will be significant only when the compact weakens to a point where shape distortion can occur.

ACKNOWLEDGMENTS

This research was supported by the National Science Foundation under Grant No. DMR-9610280 and the National Aeronautics and Space Administration under Grant No. NAG 3-1287.

REFERENCES

1. S.R. Broadbent and J.M. Hammersley: *Percolation Processes, Proceedings of the Cambridge Philological Society,* 1957, vol. 53, pp. 629-45.
2. R.M. German: *Metall. Mater. Trans. A,* 1997, vol. 28A, pp. 1553-67.
3. R.M. German: *Liquid Phase Sintering*, Plenum Press, New York, NY, 1985.
4. K.S. Hwang, R.M. German, and F.V. Lenel: *Metall. Trans. A,* 1987, vol. 18A, pp. 11-17.
5. J.L. Johnson, A. Upadhyaya, and R.M. German: *Metall. Mater. Trans. B,* 1998, vol. 29B, pp. 857–66.
6. C.M. Kipphut, A. Bose, S. Farooq, and R.M. German: *Metall. Mater. Trans. A,* 1988, vol. 19A, pp. 1905-13.
7. R.M. German: *Advances in Powder Metallurgy,* Metal Powder Industries Federation, Princeton, NJ, 1991, vol. 4, pp. 183-94.
8. R. Raman and R.M. German: *Metall. Mater. Trans. A,* 1995, vol. 26A, pp. 653-59.
9. R.M. German: *Metall. Mater Trans. A,* 1995, vol. 26A, pp. 279-88.
10. C.M. Kipphut, T. Kishi, and R.M. German: *Progress in Powder Metallurgy,* Metal Powder Industries Federation, Princeton, NJ, 1987, vol. 43, pp. 93-106.
11. S.S. Mani and R.M. German: *Advances in Powder Metallurgy,* Metal Powder Industries Federation, Princeton, NJ, 1991, vol. 4, pp. 195-212.
12. C.M. Kipphut, A. Bose, T. Kishi, and R.M. German: *Advances in Powder Metallurgy,* Metal Powder Industries Federation, Princeton, NJ, 1989, vol. 2, pp. 415-29.
13. D. Heaney, R.M German, and I. Ahn: *Advances in Powder Metallurgy,* Metal Powder Industries Federation, Princeton, NJ, 1993, vol. 2, pp. 169-80.
14. G. Deutscher, R. Zallen, and J. Adler: *Percolation Structures and Processes,* Adam Hilger, Bristol, United Kingdom, 1983.
15. M. Sahini: in *The Mathematics and Physics of Disordered Media*, Series of Lecture Notes in Mathematics, B.D. Hughes and B.W. Ninham, Springer-Verlag, Berlin, NY, Minneapolis, MN, 1983. vol. 1035, pp. 314-46.
16. A. Bunde and S. Havlin: *Fractals and Disordered Systems*, Springer, Berlin, 1991.
17. D. Stauffer and A. Aharony: *Introduction to Percolation Theory,* 2nd ed., Taylor & Francis Ltd., London, 1992.
18. B.D. Hughes: *Random Environments and Random Walks*, Oxford University Press, London, 1993.
19. P.J. Flory: *J. Am. Chem. Soc.*, 1941, vol. 63, pp. 3083-90.
20. W.H. Stockmayer: *J. Chem. Phys.*, 1943, vol. 11, pp. 45-55.
21. M. Sahimi: *Applications of Percolation Theory,* Taylor & Francis Ltd., London, 1994.
22. S. Redner: in *The Mathematics and Physics of Disordered Media*, Series of Lecture Notes in Mathematics, B.D. Hughes and B.W. Ninham, eds., Minneapolis, MN, 1983, Springer-Verlag, Berlin, NY, vol. 1035, pp. 184-200.
23. B.J. Last and D.J. Thouless: *Phys. Rev. Lett.*, 1971, vol. 27, pp. 1719-21.
24. I. Balberg: *Phil. Mag.*, 1987, vol. B56, pp. 991-1003.
25. U. Alon, I. Balberg, and A. Drory: *Phys. Res. Lett.*, 1990, vol. 66, pp. 1879-2882.
26. A. Drory, I. Balberg, U. Alon, and B. Berkowitz: *Phys. Rev.*, 1991, vol. A43, pp. 6604-12.
27. H. Scher and R. Zallen: *J. Chem. Phys.*, 1970, vol. 53, pp. 3759-61.
28. V.K.S. Shante and S. Kirkpatrick: *Adv. Phys.*, 1971, vol. 20, pp. 325-57.
29. G.R. Jerauld, L. E. Scriven, and H.T. Davis: *J. Phys.*, 1984, vol. C17, pp. 3429-39.
30. R.M. German: *Sintering Theory and Practice,* Wiley-Interscience, New York, NY, 1996, pp. 255-58.
31. F.V. Lenel, H.H Hausner, E. Hayashi, and G.S. Ansell: *Powder Metall.*, 1961, vol. 8, pp. 25-36.
32. F.V. Lenel, H.H. Hausner, A.E. Shanshoury, J.G. Early, and G.S. Ansell: *Powder Metall.*, 1962, vol. 10, pp. 190-98.
33. F.V. Lenel, H.H. Hausner, O.V. Roman, and G.S. Ansell: *Trans. TMS-AIME*, 1963, vol. 227, pp. 640-44.
34. J. Liu, Y. Liu, A. Lal, and R. M. German: *Scripta Metall.*, 1999, vol. 40, pp. 1221-27.
35. W.D. Klopp and P.L. Raffo: "Effects of Purity and Structure on Recrystallization, Gain Growth, Ductility, Tensile and Greep Properties of Arc-Melted Tungsten," NASA-TND-2503, Lewis Research Center, Cleveland, OH, 1964.
36. A. Upadhyaya: Ph.D. Thesis, Pennsylvania State University, University Park, PA, 1998.
37. R.M. German: *Metall. Trans. A,* 1985, vol. 16A, pp. 1247-52.